Polymer 50 (2009) 4378–4388

Contents lists available at ScienceDirect

Polymer

journal homepage: www.elsevier.com/locate/polymer

Polymorphic crystallization of fractionated microbial medium-chain-length polyhydroxyalkanoates

Sisi Chen [a,b,1], Qian Liu [c,1], Honghui Wang [c], Bo Zhu [b], Fang Yu [b], Guo-Qiang Chen [a,c,*], Yoshio Inoue [b,**]

[a] Department of Biological Sciences and Biotechnology, Tsinghua University, Beijing 100084, China
[b] Department of Biomolecular Engineering, Tokyo Institute of Technology, 4259-B-55 Nagatsuta, Midori-ku, Yokohama 226-8501, Japan
[c] Multidisciplinary Research Center, Shantou University, Shantou 515063, Guangdong, China

ARTICLE INFO

Article history:
Received 31 March 2009
Received in revised form
18 June 2009
Accepted 7 July 2009
Available online 23 July 2009

Keywords:
PHB
PHA
Crystallization

ABSTRACT

By focusing on a range of fractions of medium-chain-length polyhydroxyalkanoates (mcl-PHA), a more in-depth understanding of the thermal properties and the crystalline structure has been gained. Dual-mode melting was observed for all the fractionated samples. Further DSC analysis revealed that such phenomenon was due to the presence of two crystalline phases (phase I and phase II), forming at different temperatures. As noted, for the samples with higher 3-hydroxytetradecanoate (HTD) comonomer composition, the crystallization rate of phase II was much depressed, which made phase I dominant. The WAXD and FTIR results indicate that the two phases differ in the crystalline structure. The in situ IR and WAXD registrations indicate that phase I would transform into phase II through a melting-recrystallization process during heating. The high similarity of IR spectra in the range of 1500–900 cm^{-1} between phases I and II excludes the possibility of adopting different conformation. It is suggested that major differences between the two crystalline phases lie in the molecular packing.

1. Introduction

Polyhydroxyalkanoates (PHA) are a family of biodegradable and biocompatible polyesters that can be produced by a variety of bacteria [1–3]. PHA have attracted much attention as biodegradable plastics and potential tissue engineering materials [4–6]. Medium-chain-length PHA (mcl-PHA) consisting of comonomer units of 3-hydroxyhexanoate (HHx), 3-hydroxyoctanoate (HO), 3-hydroxydecanoate (HD), 3-hydroxydodecanoate (HDD), 3-hydroxytetradecanoate (HTD), or even longer-chain comonomer units have been recently synthesized by *Pseudomonas putida*, a well-known mcl-PHA producer [7–9].

Biologically synthesized PHA have been shown to have a broad chemical compositional distribution (CCD) [10]. For example, It was reported by Erik et al. that PHA synthesized by *Cupriavidus necator* were blends of poly(3-hydroxybutyrate) (PHB) and random copolymer of 3-hydroxybutyrate and 3-hydroxyvalerate (PHBV) [11]. With a fractionation technique, PHA were separated into fractions containing narrow property distributions [12]. Generally, these fractions showed significantly different thermal properties, and it was found that properties of PHA copolymers depend strongly on the distribution of comonomer unit composition and molecular weight [13].

It has been widely accepted that mcl-PHA show amorphous and elastic properties with a lower melting point (T_m) and a lower degree of crystallinity compared with short-chain-length PHA (scl-PHA) [14–17]. Interestingly, recent study demonstrated that the presence of over 30% long chain comonomer units such as HDD and HTD in the mcl-PHA increased the T_m and the degree of crystallinity of mcl-PHA, leading to dramatic changes in mcl-PHA mechanical properties [8,9] making them significantly different from those of the typical mcl-PHA.

So far, no reasonable explanation was provided for this phenomenon. In addition, conclusions regarding the mcl-PHA containing high proportion of HDD and HTD were all drawn from the analysis of original biosynthesized mcl-PHA, which could be blends of various PHA with various properties. Therefore, it is necessary to study these original mcl-PHA excluding possible blends.

It has been known that both the primary structure, including chemical structure and comonomer-unit composition [18,19], and the solid-state play a significant role in determining polymer biodegradability. The solid-state of PHA includes many factors, such as the degree of crystallinity [20,21], lamellar thickness, the

* Corresponding author. Department of Biological Sciences and Biotechnology, Tsinghua University, Beijing 100084, China. Tel.: +86 10 6278 3844; fax: +86 10 6279 4217.
** Corresponding author. Tel.: +81 45 924 5794; fax: +81 45 924 5827.
E-mail addresses: chengq@mail.tsinghua.edu.cn (G.-Q. Chen), inoue.y.af@m.titech.ac.jp (Y. Inoue).
[1] These authors contributed equally to this paper.

0032-3861/$ – see front matter © 2009 Elsevier Ltd. All rights reserved.
doi:10.1016/j.polymer.2009.07.011

conformation and conformational flexibility of chains in the crystalline phase as well as the chain packing. It is easy to understand the effects of chain packing and conformation on the PHA biodegradation, as the enzymatic degradation occurs through hydrolyzing ester linkages of PHA main chains. However, only limited results are available on this subject till now. Therefore, it is necessary to develop the basic understanding of crystalline structures of PHA.

In the present study, mcl-PHA containing high proportions of HDD and HTD were successfully fractionated using mixed solvents of chloroform/ethanol. The comonomer unit compositional distribution and thermal properties of the original biosynthesized mcl-PHA samples and their series of fractions were studied. The crystallization kinetics were investigated using differential scanning calorimetry (DSC), while the crystalline structures were studied by the wide angle X-ray diffraction (WAXD) and time-resolved Fourier transform infrared spectroscopy (FTIR). In addition to the DSC results, the temperature-dependent WAXD and temperature-dependent FTIR were used to monitor the polymorphic behavior of mcl-PHA during the crystallization and melting process.

2. Experimental materials

Three mcl-PHA samples with the number-average molecular weight (M_n) of 5.85×10^4, 4.15×10^4, and 3.38×10^4 were biosynthesized by *P. putida* KTOY06 [9], a β-oxidation pathway weakened mutant strain from a well-known mcl-PHA producer *P. putida* KT2440 [22,23]. Tetradecanoic acid was used as a sole carbon source. The details of biosynthesis of these mcl-PHA samples were reported elsewhere [8]. All the original samples were found to consist of five comonomer units (HHx, HO, HD, HDD and HTD), while their comonomer unit compositions were different from each other.

2.1. Fractionation

The as-produced mcl-PHA samples denoted as "original" samples, were fractionated by mixed solvents of chloroform/ethanol as indicated below. The original mcl-PHA samples were dissolved in chloroform at a polymer concentration of 10 g/L. Ethanol was then slowly added into the polymer/chloroform solution under gentle agitation at ambient temperature until precipitates were visually observed. The mixed solution was maintained at 4 °C for 24 h. Subsequently, the precipitated substance was isolated by centrifugation at 9000 rpm for 30 min. The precipitates obtained were transferred to a Petri dish and dried under vacuum at 28 °C for 48 h. This procedure was repeated until the addition of a large amount of ethanol could not cause appreciable precipitation. The last fraction was obtained by evaporating the residue solvent.

2.2. Characterization of physical properties

2.2.1. Gel permeation chromatography (GPC)

Molecular weights of the mcl-PHA polymer samples were studied on an HLC-8020 GPC system (Tosoh Co., Tokyo, Japan) assembled with GEL G2000Hxl and GMHxl columns (TSK). Chloroform was used as an eluent at a flow rate of 1.0 ml/min. Polystyrene standards with narrow molecular distribution were used to calibrate the GPC elution curve. Number-average (M_n) and weight-average (M_w) molecular weights as well as the polydispersity index (M_w/M_n) of original and fractionated samples were calculated through a SC-8010 data processor.

2.2.2. Gas chromatography (GC)

Comonomer compositions of mcl-PHA were determined after methanolysis of the polymer samples using gas chromatography (GC) on a Shimadzu GC-17A (Kyoto, Japan) equipped with an InertCap 1 capillary column (30 m by 0.25 mm) (GL Sciences, Tokyo, Japan) and a flame-ionization detector.

2.2.3. Carbon nuclear magnetic resonance (^{13}C NMR)

Solution ^{13}C NMR spectra were recorded on a 600 MHz/54 mm NMR spectrometer (Bruker Ultrashield Co., Tokyo, Japan) under ambient temperature. $CDCl_3$ was used as the solvent and the chemical shift reference.

2.2.4. Differential scanning calorimetry (DSC)

The melt-crystallization and melting behavior of the samples were studied on a Pyris Diamond DSC (Perkin-Elmer, Japan, Yokohama, Japan). Firstly, the cast samples were heated from −50 °C/min to 100 °C at a scanning rate of 10 °C/min to evaluate the melting behavior. After maintaining at 100 °C for 1 min, the samples were cooled to −50 °C at a scanning rate of 10 °C/min to observe the non-isothermal crystallization. Then the samples were re-heated from −50 to 100 °C at 10 °C/min to observe the melting behavior. The melting behaviors of non-isothermally crystallized samples at different heating rates and non-isothermal crystallization behaviors at different cooling rates were also studied.

2.2.5. Dynamic mechanical thermal analysis (DMTA)

Dynamic mechanical thermal analysis system DMS210 with SSC5300 controller (Seiko Instrument Co. Ltd, Tokyo, Japan), was utilized to measure the T_g value. The frequency of the oscillation force was maintained at 0.5 Hz and the samples were treated at a heating rate of 2 °C/min.

2.2.6. Fourier transform infrared spectroscopy (FTIR)

The transmission IR spectra were measured on an AIM-8800 (Shimadzu Co., Japan), equipped with an IMV-4000 multichannel infrared microscope (Shimadzu Co., Japan) and an MCT detector in the transmission mode. Mcl-PHA sample was placed between two pieces of BaF_2 slides, and then it was melted at 100 °C for 2 min in an LK-600FTIR hot stage (Linkam Scientific Instruments Ltd, Surrey, UK) equipped with a cooling unit (L600A) under the protection of dry nitrogen gas. The amorphous sample was then quenched to selected temperature by a flow of liquid nitrogen for isothermal melt-crystallization. Afterward, the isothermally crystallized samples were re-heated at 1 °C/min and the spectral changes were also monitored.

2.2.7. Wide angle X-ray diffraction (WAXD)

The temperature-dependent WAXD measurement was recorded on a Bruker D8 ADVANCE diffractometer at a scanning rate of 4 °/min ($\lambda = 1.54$ Å, 40 KV and 40 mA). The samples were hot pressed at 100 °C for 1 min, and then quenched to a pre-selected temperature, followed by maintaining at that temperature for 24 h to allow a complete crystallization. WAXD data were collected over a temperature range from 28 °C to 80 °C in the scattering angle range of $2\theta = 12–30$ °. The degree of crystallinity was calculated from the data processing software on the basis of Vonk method [24]. The samples used for measuring the degree of crystallinity were dissolved first in chloroform as a solvent and then recovered from the solution by casting. Before measurement, these samples were annealed for one week at 28 °C.

3. Results and discussion

3.1. Fractionation of mcl-PHA

The as-produced mcl-PHA with M_n of 5.85×10^4, 4.15×10^4 and 3.38×10^4 were denoted as A, B, and C-original, respectively.

Bacterial mcl-PHA were fractionated into several fractions by the precipitation method using a mixed solvent of chloroform/ethanol. As shown in Table 1, HO composition of the fractionated mcl-PHA increased gradually for all original samples, while HTD composition decreased as the concentration of ethanol increased. The HD composition increased gradually for B and C fractions. The HDD composition in both the original samples and the fractions were similar to each other, and the HHx composition was very low. In addition, the M_n of almost all fractions (except for B-1 and C-1 fractions) decreased gradually as the concentration of ethanol increased.

According to a previous study [25], the comonomer compositional fractionation of P(3HB-*co*-3HA) by chloroform/*n*-heptane mixed solvent depends normally on the length of the side chain and the composition of comonomer units. In our experiments, fractionation of mcl-PHA was found to depend on both the comonomer composition and the molecular weight. Usually the fractions precipitated earlier had both higher HTD composition and higher averaged molecular weight, although fractions with relatively low M_n but extremely high HTD content (fractions B-1 and C-1) could also be precipitated earlier. The influence of comonomer composition on the solubility of mcl-PHA in ethanol could be explained by the effects of comonomer composition to molecular polarity. Higher composition of comonomer units with longer alkyl side chain (HTD) leads to a lower polarity, therefore a poorer solubility in the polar ethanol solvent. The results also indicate that the biosynthesized mcl-PHA were not compositionally uniform, they contained very board comonomer compositional and molecular weight distributions.

In Fig. 1 are shown the liquid ^{13}C NMR spectra and their assignments for the original mcl-PHA samples and their fractions. The ^{13}C NMR resonance assignment of mcl-PHA was referring to those reported previously (Fig. 1a–c) [26]. As shown by spectra of the terminal carbons of the side chain for each fraction of the B-original sample (Fig. 1c), the resonance intensity ratio of HTD-HDD terminal carbon to HD and HO terminal carbon was higher in the earlier precipitates from the B-original sample. This result agreed with that of GC's. Results of A and C samples were similar to that of B sample and were not shown here.

3.2. Thermal properties of mcl-PHA

To investigate the effects of composition distribution on the physical properties of mcl-PHA, DSC thermograms were measured. Samples were dissolved first in chloroform as a solvent and then recovered from the solution by casting. These samples were annealed for one week at 28 °C prior to DSC and WAXD studies. Fig. 2 presents the first DSC heating scans of the cast mcl-PHA samples. Fusion enthalpy (ΔH_m) of A-original sample was 32.6 J/g, with a degree of crystallinity of 43.9% measured by WAXD (diffraction data not shown here). For the fractions, the value of ΔH_m calculated from the total area of all endothermic peaks increased from 30.2 to 35.5 J/g, and the degree of crystallinity slightly increased from 43.2% to 45.2% with the increasing of HTD composition. The B- and C-original samples and their fractions revealed similar trends. It was reported by Liu et al. [8] and Ouyang et al. [9] that mcl-PHA with a high long side-chain comonomer composition behaved differently in their thermal properties compared with the mcl-PHA containing less than 10% HDD or HTD. The latter normally have decreased crystallinity and increased elasticity due to the presence of long alkyl side-chains [27,28]. In the present study, results were further classified by the fractionated samples. It was interesting to note that mcl-PHA with higher HTD composition showed a similar (or even a higher) degree of crystallinity by WAXD and DSC compared with those with lower HTD composition. Normally, for the random copolymer, incorporation of a foreign comonomer disturbs the order of a polymer, leading to a sharp decrease in the degree of crystallinity. The dependence of the degree of crystallinity of mcl-PHA on its HTD comonomer composition implies that the long side chain will also be involved in the crystallization process in the mcl-PHA consisting of high content of long chain comonomer such as HTD.

On the other hand, it is of note that dual melting behavior was observed in this study, which is different from the previous results [8,9]. As shown in Fig. 2, the A-original sample showed a broad endothermic peak with its top at about 57.1 °C. In comparison with the A-original sample, its fractions showed two melting peaks (T_{m1} and T_{m2}). The position and the area of the two melting peaks were significantly influenced by the HTD composition. Samples with

Table 1
Molecular weights and comonomer composition of mcl-PHA and their fractions.

Fraction no.	Ethanol conc. (%)	Subtraction (wt.-%)	M_n (10^{-4})[a]	M_n/M_w[a]	PHA polymer monomer composition (mol%)[b]				
					HHx	HO	HD	HDD	HTD
A-original	–	–	5.85	1.9	1.7	14.7	27.3	32.8	23.6
A-1	66	17.2	8.59	1.4	0.9	10.5	26.3	34.7	27.6
A-2	70	16.8	7.66	1.5	0.9	12.9	30.1	33.8	22.2
A-3	73	14.1	6.06	1.6	1.7	16.6	30.7	30.5	20.5
A-4	75	15.1	3.79	1.5	2.1	15.7	28.0	34.0	20.2
A-5	78	15.2	3.33	1.4	2.0	18.0	29.7	33.7	16.6
A-6	81	4.7	3.14	1.4	2.7	22.1	32.8	33.1	9.3
A-7[c]	–	16.9	1.65	1.4	2.1	17.9	32.6	31.0	16.3
B-original	–	–	4.15	1.8	1.3	14.1	29.9	31.9	22.8
B-1	67	27.1	4.45	2.0	0.4	6.2	22.2	31.0	40.2
B-2	74	22.5	6.7	1.5	1.2	15.1	34.7	27.0	22.1
B-3	78	21.5	4.67	1.7	1.6	17.7	36.6	25.0	19.2
B-4	81	15.1	3.73	1.5	1.2	17.7	36.3	26.2	18.6
B-5[c]	–	13.8	2.4	1.3	1.7	20.4	38.5	23.9	15.5
C-original	–	–	3.38	1.8	0.3	7.7	30.4	34.8	26.8
C-1	68	37.5	3.39	2.0	0.2	3.8	21.1	32.0	43.0
C-2	72	36	3.89	1.8	0.9	11.6	35.9	34.5	17.2
C-3	78	10.8	2.41	1.6	0.3	10.6	36.2	38.6	14.4
C-4[c]	–	15.7	2.07	1.7	0.5	13.0	42.2	36.1	8.3

[a] Determined by GPC.
[b] Determined by GC.
[c] A-7, B-5 and C-4 fractions were obtained by evaporating the solvent from the solution after fractionation of A-6, B-4 and C-3, respectively.

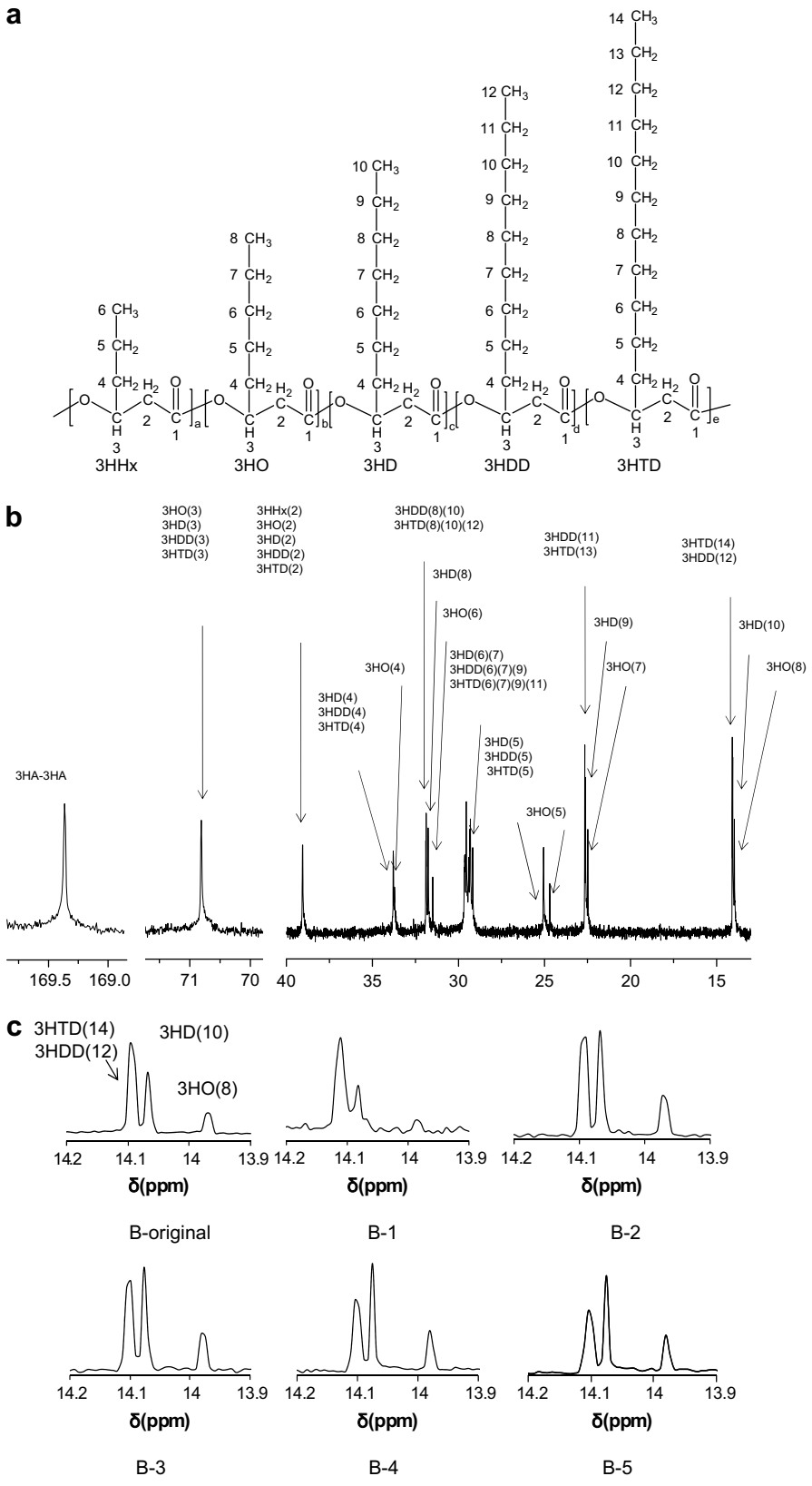

Fig. 1. (a) Molecular structure of mcl-PHA. (b) ^{13}C NMR spectra of the A-1 mcl-PHA sample. (c) ^{13}C NMR resonance of the terminal carbon for the fractions of B-original mcl-PHA sample.

higher HTD composition showed higher melting temperatures of these two peaks. Furthermore, the T_{m1} peak was found to be higher in its enthalpy magnitude with respect to the T_{m2} one for the samples with higher HTD composition. The dual melting peaks were also detected for the B- and C-original samples and their fractions. Such dual melting behavior will be discussed later.

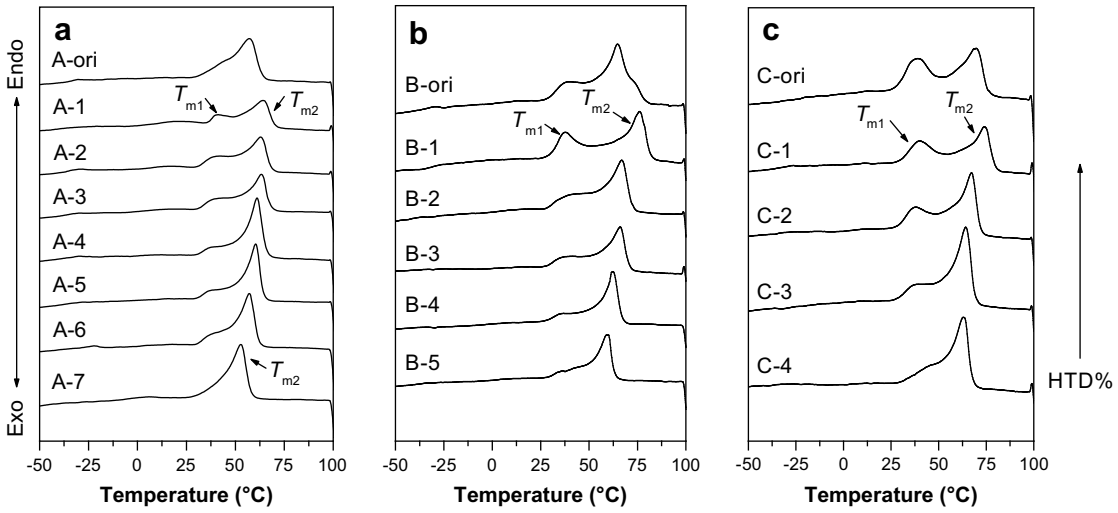

Fig. 2. The 1st DSC heating scans for the cast original mcl-PHA samples and their fractions at a heating rate of 10 °C/min.

T_g was measured by DMTA, which is considered as one of the most sensitive method for measuring glass transition temperature. All the original samples and their fractions have an approximately constant T_g at around −42 °C, similar to the previously reported values [8], suggesting that the comonomer composition did not influence the T_g in the case samples of mcl-PHA copolymers.

3.3. Nonisothermal melt-crystallization and melting behavior

The mcl-PHA samples showed two melt-crystallization peaks (T_{c1} and T_{c2}) during the cooling process (Fig. 3 and Table 2). Samples with higher HTD composition showed higher crystallization temperatures of these two peaks. Furthermore, the T_{c1} peak was found to be higher in its enthalpy magnitude with respect to the T_{c2} one for the samples with higher HTD composition, indicating that mcl-PHA with higher HTD composition preferred to crystallize at T_{c1}. The subsequent melting traces were also registered for the non-isothermally crystallized samples. As shown in Fig. 4, their melting normally presents two melting peaks (T_{m1} and T_{m2}), which are divided by a cold crystallization (T_{cc2}). The enthalpy of T_{m1} was found to increase with the HTD composition, while the enthalpy of T_{m2} decreased obviously. The dependence of the crystallization enthalpy on the HTD composition was compared to that of the melting enthalpy. Clearly, the enthalpy of T_{m1} accords with that of T_{c1}, even without considering the loss from cold crystallization. Meanwhile, the enthalpy of T_{m2} turns out to be the sum of enthalpy of T_{c2} and T_{cc2}. All the results above implied that the two melting peaks T_{m1} and T_{m2} arouse from two crystalline phases which crystallize at T_{c1} and T_{c2}, respectively (named here as crystalline phases I and II). These two phases showed different crystallization kinetics during the cooling process, with the magnitudes of the two crystalline peaks strongly affected by HTD comonomer composition.

It is interesting to notice that higher HTD composition favored the formation of crystalline phase I during the cooling process, and lower HTD composition favored the other. As shown in Fig. 3c, fractions with lower HTD composition are able to crystallize mainly as the crystalline phase II when the cooling rate is 10 °C/min, while the fractions with higher HTD composition (e.g. C-1 fraction) were observed to mainly crystallize at peak T_{c1} when cooled at 10 °C/min. However, as the cooling rate decreased to 2 °C/min, the peak T_{c1} almost disappeared, while the magnitude of peak T_{c2} was greatly

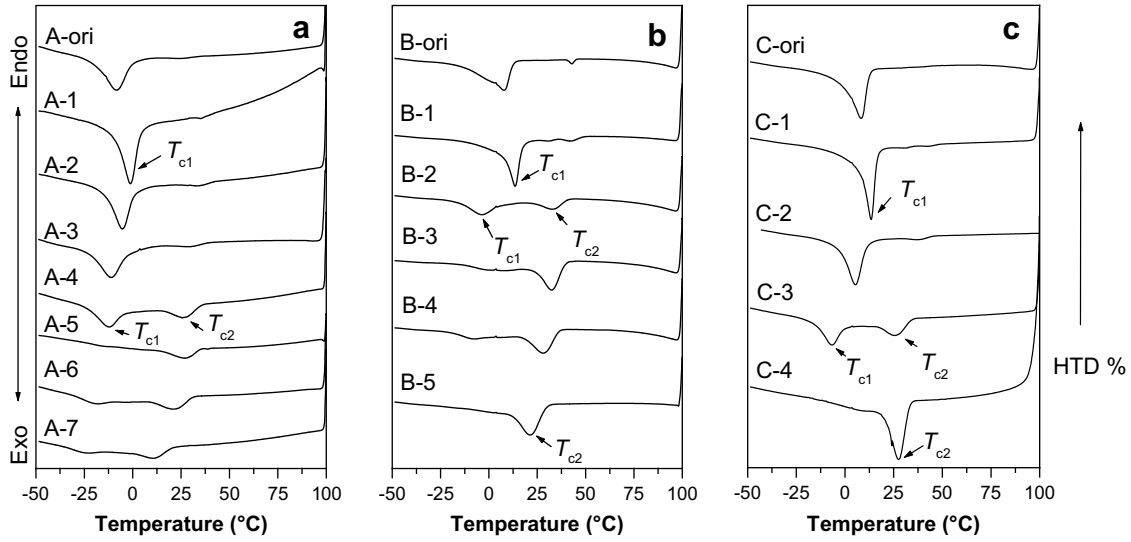

Fig. 3. The DSC cooling scans at a cooling rate of 10 °C/min for the original mcl-PHA samples and their fractions after melted at 100 °C.

Table 2
Thermal properties of original and fractionated bacterial mcl-PHA.

Fraction No.	HTD fraction (mol %)	T_{m1}[a] (°C)	T_{m2}[a] (°C)	T_g[b] (°C)	ΔH_m[a] (J/g)	T_{c1}[a] (°C)	T_{c2}[a] (°C)	Crystallinity[c] (%)
A-original	23.6	–	57.1	−42.6	32.6	−8.4	–	43.9
A-1	27.6	39.8	64.1	−42.7	35.5	−1.2	–	45.2
A-2	22.2	38.8	62.8	−42.6	34.7	−5.3	–	44.7
A-3	20.5	38.7	63.3	−43.2	33.2	−11.0	28.6	42.2
A-4	20.2	36.6	61.1	−43.7	32.9	−12.2	26.5	44.1
A-5	16.6	35.7	60.1	−42.5	31.3	−12.1	26.5	43.6
A-6	9.3	35.7	57.1	−41.9	30.2	−17.7	20.9	43.2
A-7	16.3	–	52.8	−40.1	29.5	−23.0	10.3	37.0
B-original	22.8	37.0	64.6	−41.0	38.5	7.8	–	45.0
B-1	40.2	37.8	76.1	−38.8	43.2	13.6	41.9	48.3
B-2	22.1	37.5	68.0	−42.5	39.1	−3.5	32.8	46.5
B-3	19.2	36.9	67.0	−41.9	36.7	–	32.4	46.3
B-4	18.6	35.3	62.1	−40.9	36.5	–	28.0	44.1
B-5	15.5	–	59.6	−42.8	32.6	–	21.3	42.6
C-original	26.8	39.1	69.6	−40.5	35.8	8.3	–	46.5
C-1	43.0	40.2	73.9	−43.7	42.3	13.4	–	50.0
C-2	17.2	37.3	67.1	−42.2	37.8	5.3	37.1	43.7
C-3	14.4	36.5	64.2	−41.1	37.0	−6.6	27.0	–
C-4	8.3	–	63.1	−42.5	33.5	–	27.5	–

[a] T_{m1}, the lower-temperature-side melting point; T_{m2}, the higher-temperature-side melting point; ΔH_m apparent heat of fusion, calculated from the total area of two endothermic curves; T_{c1},the lower crystallization temperature; T_{c2},the higher crystallization temperature.
[b] T_g was determined by DMTA.
[c] The degree of crystallinity was determined by WAXD.

enhanced, indicating that the crystalline phase II became dominant (Fig. 5). Besides, although the fractions with high HTD composition (e.g. C-1 fraction) hardly showed any cold crystallization peak in the subsequent heating curves at 10 °C/min after the non-isothermally crystallization process (Fig. 4c), significant cold crystallization peak T_{cc2} and the following melting peak T_{m2} could be observed (Fig. 6) when the heating rate was decreased to 2 °C/min. This phenomenon indicates that the fractions with higher HTD composition were able to crystallize as the crystalline phase II as well as those with lower HTD composition but at a lower crystallization rate.

It turns out that the crystallization kinetic of the crystalline phase II is strongly affected by the comonomer composition. The mcl-PHA with high HTD composition normally crystallize at much depressed rate at T_{c2}. Such phenomenon reveals the reason why mcl-PHA with higher HTD composition mainly crystallized in phase I during the cooling process. It also indicates that, by controlling the thermal procedures, we were able to prepare the mcl-PHA samples with one crystalline phase only (phase I or II).

3.4. Polymorphic crystallization of mcl-PHA

A varies of explanations, e.g., multiple nucleation, polymorphic crystallization, etc., could be available for the dual-mode crystallization. To further reveal the driving forces for the dual-mode crystallization of mcl-PHA, the WAXD measurements were employed to investigate the crystalline structure of the two crystalline phases. The mcl-PHA samples crystallized in the two crystalline phases were obtained by adjusting the thermal procedure as described below. The C-1 sample was firstly hot pressed at 100 °C for 2 min to erase the residual thermal history, and subsequently quenched to 58 and 28 °C directly to isothermally crystallize into crystalline phases II and I, respectively, followed by maintaining at that temperature for 24 h to allow a complete crystallization. The WAXD spectra of the two samples with different crystalline phases are compared in Fig. 7. Clearly, the crystalline phase II shows two major diffractions at 19.3° and 21.5°. In the case of the crystalline phase I, however, a new diffraction at 19.8°, which contributes most

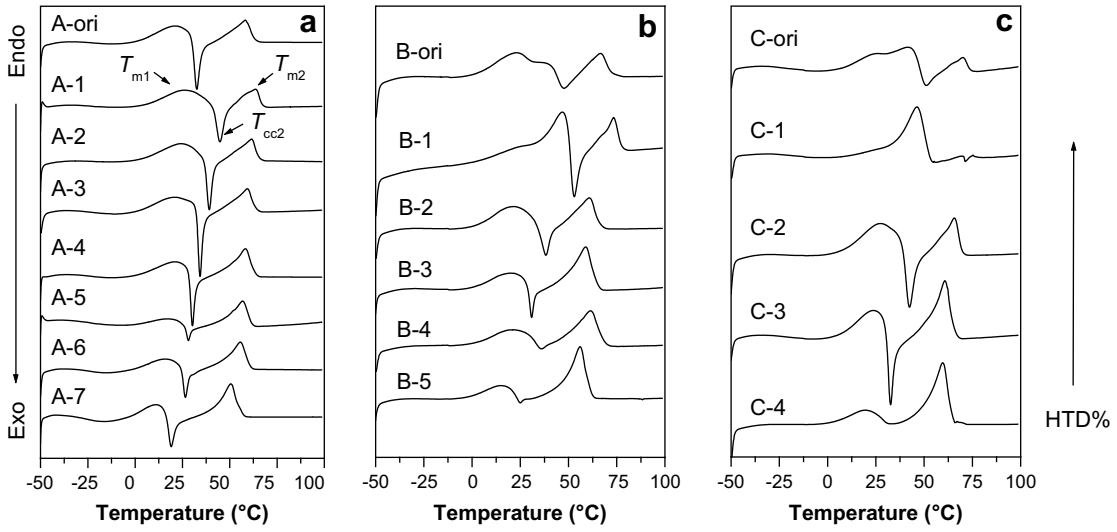

Fig. 4. The subsequent DSC heating scans at a heating rate of 10 °C/min for the samples crystallized during the cooling procedure showed in Fig. 3.

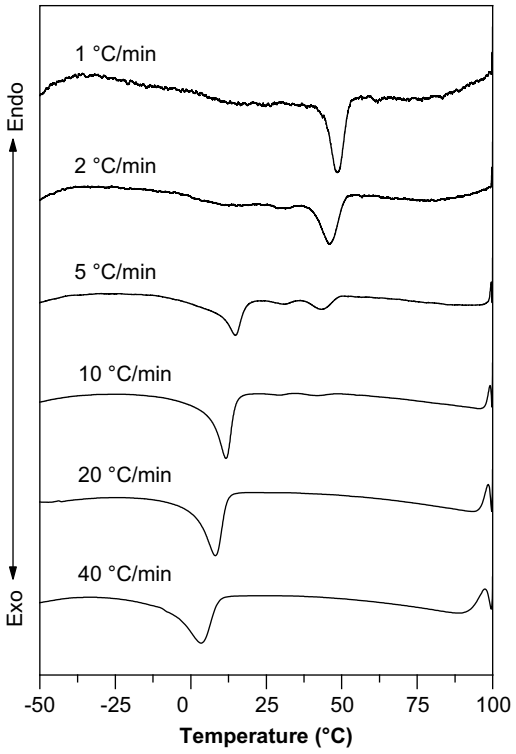

Fig. 5. DSC cooling scans varied from 1 °C/min to 40 °C/min for the C-1 fraction sample after melted at 100 °C.

of diffraction, was detected instead. The differences in the WAXD pattern, which could be observed more clearly in the *in situ* X-ray registration during melting (shown later), indicate that the two phases were enrolled into two different crystalline structures.

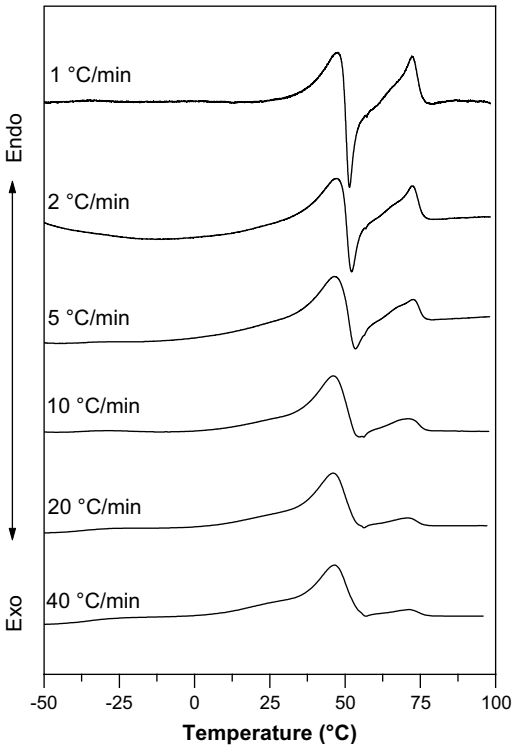

Fig. 6. The subsequent DSC heating scans varied from 1 °C/min to 40 °C/min for the C-1 fraction sample crystallized during the cooling procedure showed in Fig. 4.

IR is very sensitive to the small changes of the conformation and the packing of polymers [29], and the in situ monitoring of the selected crystal growth was expected to shed light on the unique crystallization of mcl-PHA. For IR experiments the C-1 sample was also melted first at 100 °C to erase the residual thermal history, and subsequently quenched to 58 and 28 °C directly for crystallization. Then *in situ* FTIR measurements were performed to monitor the isothermal crystallization of crystalline phase II and phase I. Fig. 8a and b show the time-resolved FTIR spectra in the C=O stretching region during the crystallization of crystalline phases II and I. During the crystallization of crystalline phase II, the intensity of the band at 1725 cm^{-1} increased gradually over time, while that of the band at 1744 cm^{-1} decreased (Fig. 8a). Therefore it is rational to assign the 1725 cm^{-1} band to the crystalline phase, while the 1744 cm^{-1} band to the amorphous phase [30]. It was reported that many types of PHA, such as PHB and PHBHHx, consisting of random 3-hydroxybutyrate (HB) and 3-hydroxyhexanoate (HHx) possess a crystalline band at this position [31–33]. Of particular interest is the fact that the crystallization of crystalline phase I gives rise to a different spectral evolution. As shown in Fig. 8b, the carbonyl stretching band of the crystalline phase I shows a 26 cm^{-1} higher frequency shift in comparison with that of crystalline phase II. The carbonyl stretching vibration is well known to be sensitive to the molecular interaction (consisting of both intra- and inter-molecular interaction), therefore, the in situ FTIR results further confirmed the existence of the two different type of crystalline structures. We also tested a few other fractions (e.g. A-1, A-7, B-1, C-2, C-4) and the results were all similar (data not shown).

3.5. Melting and phase transformation of mcl-PHA

To further confirm the polymorphic crystallization and clarify the multiply melting behaviors of mcl-PHA, the temperature-dependent WAXD patterns were registered during the melting of crystalline phase II and phase I (Figs. 9 and 10). The mcl-PHA samples crystallized in the two crystalline phases were obtained by adjusting the thermal procedure as described above. The C-1 sample was melted first at 100 °C to erase the residual thermal history, and subsequently quenched to and maintained for 24 h at 58 and 28 °C to crystallize into crystalline phases II and I, respectively. Then the samples were re-heated, and the WAXD patterns

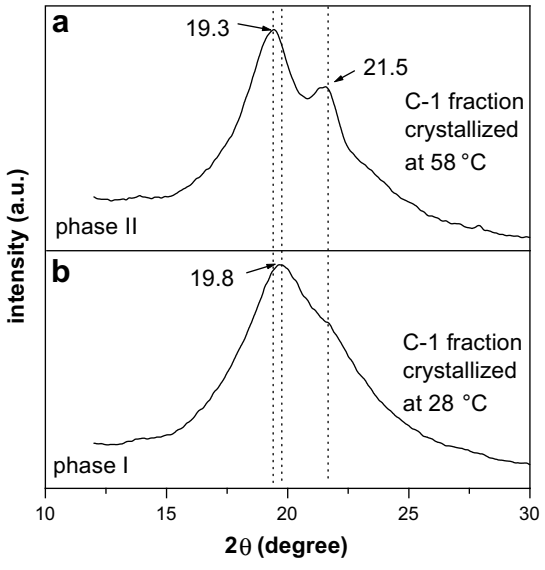

Fig. 7. WAXD patterns for the C-1 fraction sample crystallized at (a) 58 °C (phase II) and (b) 28 °C (phase I).

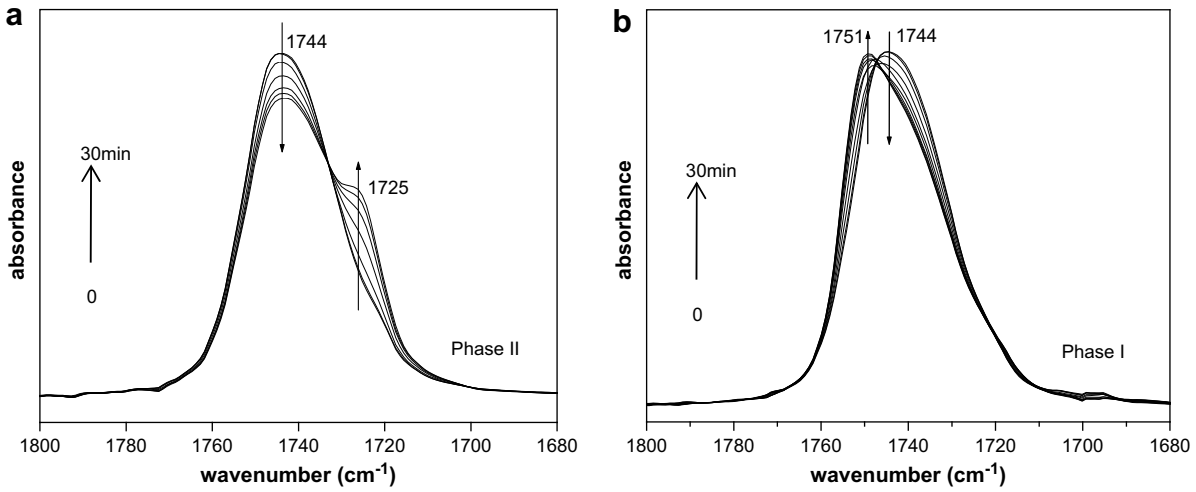

Fig. 8. Time-resolved FTIR spectra in the 1800–1680 cm^{-1} range registered during crystallization at (a) 58 °C (phase II) and (b) 28 °C (phase I) for the C-1 fraction sample.

were measured over a temperature range from 28 °C to 80 °C, in the scattering angle range of $2\theta = 12–30°$.

Fig. 9 shows the temperature dependence of the WAXD patterns during the melting process of crystalline phase II. The crystalline phase II shows two major diffraction peaks at 19.3° and 21.5°, whose intensities decreased with increasing temperature from 28 to 60 °C. The sample was found to be melted completely at 80 °C, and the amorphous C-1 sample showed one major diffraction peak at 18.5°. In the case of the crystalline phase I as shown in Fig. 10, however, the change was more complex. As temperature increased from 28 to 48 °C, the diffraction peak at 19.8° contributing most of diffraction decreased gradually in intensity. When the temperature increased above 48 °C, the dominant diffraction shifted gradually to 19.3°, which was assigned to phase II. Further, the peak at 21.5°, which also arises from phase II, was significantly enhanced with increasing temperature. After the temperature reached 60 °C, the diffraction peaks at 19.3° and 21.5° decreased gradually until the sample changed to its amorphous state. The distinctive differences among the WAXD patterns of the amorphous state, the crystalline phase II and the crystalline phase I, as kinetically revealed here, further confirm the presence of the two different crystalline structures. Moreover, it clearly shows that phase transition process occurred during the melting of the crystalline phase I. That is, during the heating process, the crystalline phase I melted and was

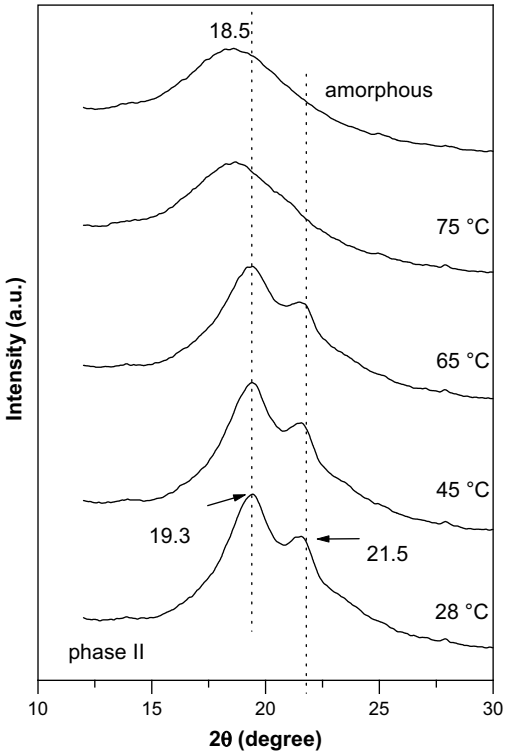

Fig. 9. Temperature-dependent WAXD patterns registered from 28 °C to 80 °C for the C-1 fraction sample crystallized at 58 °C (phase II).

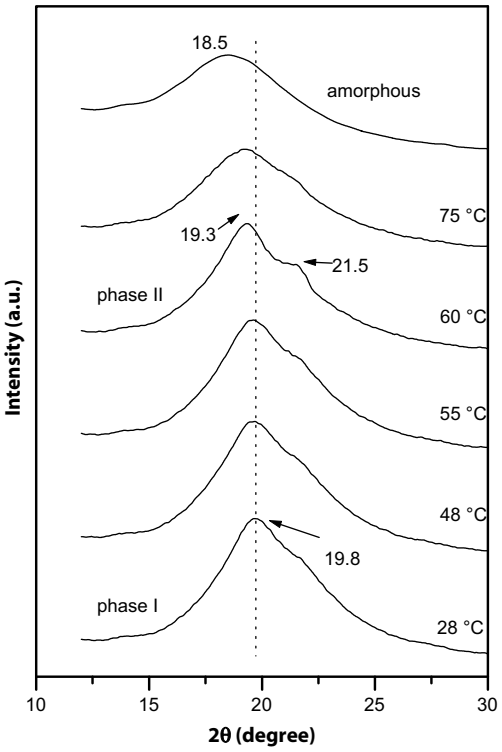

Fig. 10. Temperature-dependent WAXD patterns registered from 28 °C to 80 °C for the C-1 fraction sample crystallized at 28 °C (phase I).

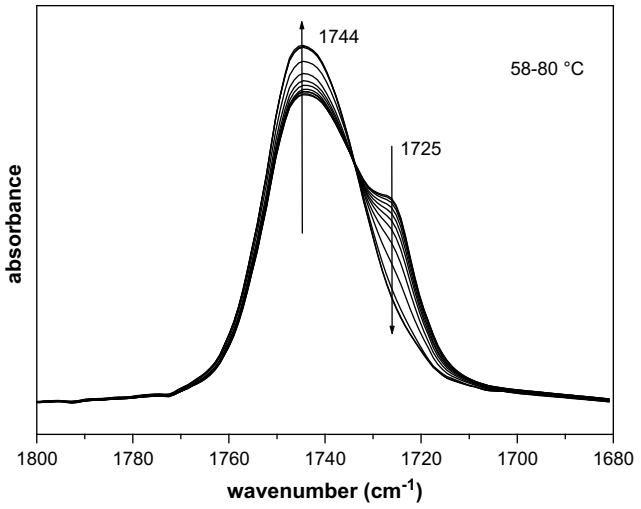

Fig. 11. Temperature-dependent FTIR spectra in the 1800–1680 cm^{-1} range registered from 58 °C to 80 °C for the C-1 fraction sample crystallized at 58 °C (phase II).

transformed into the crystalline phase II, and then the re-crystallized crystalline phase II melted at higher temperatures.

Figs. 11 and 12 present the corresponding temperature-dependent FTIR spectra during the melting process of C-1 sample crystallized in crystalline phases II and I at 1 °C/min, respectively. The C-1 sample was melted first at 100 °C and subsequently quenched to and maintained at 58 and 28 °C for 30 min to crystallize into crystalline phases II and I, respectively. Then the sample was re-heated at 1 °C/min. During the melting process of crystalline phase II, the intensity of the crystalline band at 1725 cm^{-1} decreased gradually, while that of the amorphous band at 1744 cm^{-1} increased. In the case of crystalline phase I, the crystalline band for crystalline phase I at 1751 cm^{-1} decreased gradually as the temperature increased from 28 to 50 °C, and disappeared at 50 °C. The crystalline band for crystalline phase II at 1725 cm^{-1} appeared at 48 °C and was enhanced from 48 to 60 °C. After that, the crystalline band for crystalline phase II at 1725 cm^{-1} decreased gradually in intensity and finally disappeared as the sample melted completely. Such results are well in accordance with the temperature-dependent WAXD patterns and the former DSC results (Fig. 6). Similar phase transformation behaviors were also observed for other fractions (e.g. A-1, A-7, B-1, C-2, C-4) (data not shown).

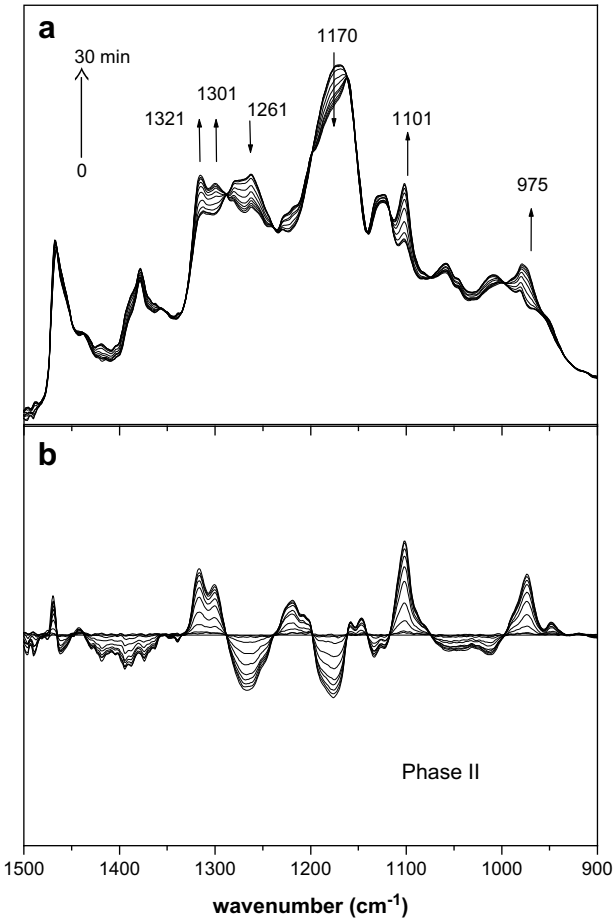

Fig. 13. (a) Time-resolved FTIR spectra in the 1500–900 cm^{-1} range registered during crystallization at 58 °C for the C-1 fraction sample (phase II) after quenched from 100 °C. (b) Difference spectra calculated by subtracting the initial amorphous spectrum from.

3.6. Discussion of conformations of phase I and phase II

As discussed above, the dual-mode crystallization of mcl-PHA was due to the presence of the two crystalline phases, which are enrolled into two difference crystalline structures. In Figs. 13 and 14 are shown the time-resolved FTIR spectra in the range of 1500–

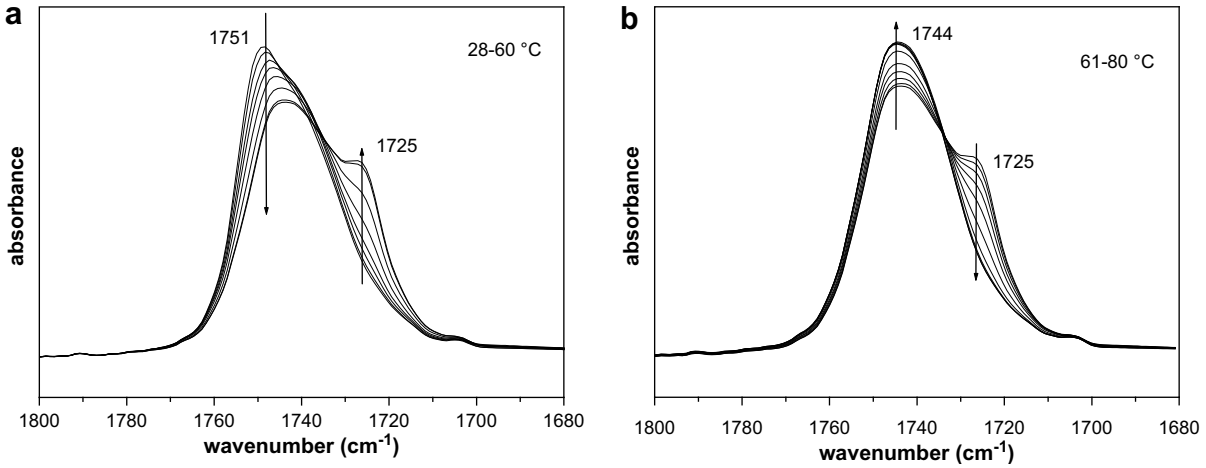

Fig. 12. Temperature-dependent FTIR spectra in the 1800–1680 cm^{-1} range registered from (a) 28 °C to 60 °C and (b) 61 °C to 80 °C for the C-1 fraction sample crystallized at 28 °C (phase I).

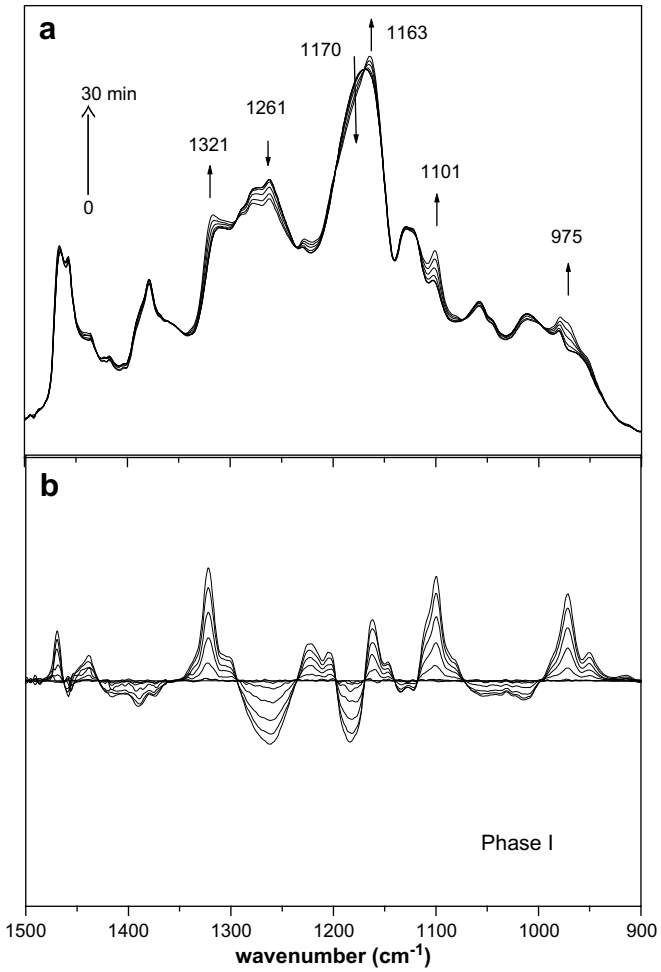

Fig. 14. (a) Time-resolved FTIR spectra in the 1500–900 cm^{-1} range registered during crystallization at 28 °C for the C-1 fraction sample (phase I) after quenched from 100 °C. (b) Difference spectra calculated by subtracting the initial amorphous spectrum from.

900 cm^{-1} of the crystalline phases II and I, respectively. On the basis of previous literature [34], the bands in the range of 1500 to 1300 cm^{-1}, 1300 to 1000 cm^{-1} and 1000–800 cm^{-1} were attributed to the CH_3, CH_2, CH bending, the C–O–C stretching and C–C backbone stretching, respectively. These bands are experimentally proved [34–37] and theoretically calculated [38] to be very sensitive to the conformational changes of backbone, both in the crystalline and amorphous phases, and were followed here to investigate the conformation evolution of mcl-PHA chains during crystallization.

The IR vibrations in the range of 1300–1000 cm^{-1}, are particularly of our interest, as they arise mainly from C–O–C backbone and should be highly sensitive to the chain conformation. The spectral vibration due to the crystallization could be clearly observed in the difference spectra shown in Figs. 13b and 14b. The band at 1170 cm^{-1} should be characteristics of the asymmetric stretching of the C–O–C group [34,39] Its intensity was noted to decrease greatly with the crystallization time and should be attributed to the amorphous chain. In contrast, the bands at 1321 and 1101 cm^{-1} showed positive intensity change with crystallization. Thus, it is reasonable to attribute the bands at 1321 and 1101 cm^{-1} to the crystalline chains. These spectral features of the two crystalline bands should reflect the conformation of the C–O–C group in the crystalline phase. As shown in Figs. 13 and 14, in the range of 1300–1000 cm^{-1}, the spectral variations induced by the crystallization process were similar between the two crystalline phases. The same results could also be observed in the whole range of 1500–900 cm^{-1}.

The high similarity of spectra in the range of 1500–900 cm^{-1} between the two phases indicates that similar chain conformation is adopted in both the two crystalline phases. With combining the observations in the C=O stretching region, it is reasonable to propose that the difference in the crystalline structure between the two crystalline phases quite possibly lies in the chain packing rather than the conformation.

4. Conclusions

Biosynthesized mcl-PHAs were fractionated into several fractions with narrow comonomer compositional distribution and molecular weight distribution. Thermal properties of mcl-PHA were analyzed. Regarding the comonomer compositions, the crystallization and melting behaviors of fractionated microbial medium-chain-length polyhydroxyalkanoates (mcl-PHA) were studied by DSC, WAXD and FTIR. The following conclusions can be reached from the present study.

The mcl-PHA samples with higher HTD composition have higher T_m and ΔH_m, indicating the capability of long side chain comonomers to crystallize.

The combination of DSC, WAXD, and IR results revealed that the mcl-PHA could crystallize into two crystalline structures, namely, phases I and II, which were temperature-dependent. It was found that the crystallization kinetic of phase II normally becomes much slower for the mcl-PHA sample with higher HTD comonomer composition. The phase transformation from phase I to phase II was detected during heating processes, and well confirmed by the *in situ* IR and X-ray registration.

The high similarity of IR spectra in the range of 1500–900 cm^{-1} between phases I and II has excluded the possibility of adopting different conformation. It is suggested that major differences between the two crystalline phases lie in the molecular packing.

Acknowledgements

Li K-Shing Foundation, the National High Tech 863 Grants (Project No. 2006AA02Z242 and 2006AA020104) and 973 Basic Research Fund (Grant No. 2007CB707804) supported this research. We are grateful to Professor Jun XU, Mr. Haimu YE (Department of Chemical Engineering, Tsinghua University) and Professor Wei MIAO (Department of Materials Science and Engineering, Tsinghua University) for their support in using the Bruker D8 ADVANCE diffractometer and interpretation of the spectra.

References

[1] Anderson AJ, Dawes EA. Microbiol Rev 1990;54:450–72.
[2] Steinbüchel A, Valentin H. FEMS Microbiol Lett 1995;128:219–28.
[3] Solaiman DK, Ashby RD, Foglia TA. Curr Microbiol 2002;44:189–95.
[4] Chen GQ, Wu Q. Biomaterials 2005;26:6565–78.
[5] Iwata T. Kagaku Keizai 2007;54:70–6.
[6] Ying T, Ishii D, Mahara A, Murakami S, Yamaoka T, Sudesh K, et al. Biomaterials 2008;29:1307–17.
[7] Sun Z, Ramsay JA, Guay M, Ramsay Ba. J Biotechnol 2007;132:280–2.
[8] Liu W, Chen GQ. Appl Microbiol Biotechnol 2007;76:1153–9.
[9] Ouyang SP, Luo RC, Chen SS, Liu Q, Chung A, Wu Q, et al. Biomacromolecules 2007;8:2504–11.
[10] Yoshie N, Inoue Y. Int J Biol Macromol 1999;25:193–200.
[11] Pederson EN, McChalicher CW, Srienc F. Biomacromolecules 2006;7:1904–11.
[12] Yoshie N, Menju H, Sato H, Inoue Y. Macromolecules 1995;28:6516–21.
[13] Noda I, Green PR, Satkowski MM, Schechtman LA. Biomacromolecules 2005;6:580–6.
[14] Nakamura S, Kunioka M, Doi Y. Macromol Rapid Commun 1991;2:15–24.
[15] Ouyang SP, Liu Q, Fang L, Chen GQ. Macromol Biosci 2007;7:227–33.
[16] Holmes PA. Phys Technol 1985;16:32–6.

[17] Ashby RD, Foglia TA, Solaiman DK, Liu CK, Nuñez A, Eggink G. Int J Biol Macromol 2000;28:355–61.
[18] Shimamura E, Scandola M, Doi Y. Macromolecules 1994;27:4429–35.
[19] Saito Y, Nakamura S, Hiramatsu M, Doi Y. Polym Int 1996;39:169–74.
[20] Koyama N, Doi Y. Macromolecules 1997;30:826–32.
[21] Spyros A, Kimmich R, Briese BH, Jendrossek D. Macromolecules 1997;30:8218–25.
[22] Kellerhals MB, Kessler B, Witholt B. Biotechnol Bioeng 1999;65:306–15.
[23] Sun Z, Ramsay JA, Guay M, Ramsay BA. Appl Microbiol Biotechnol 2007;74:69–77.
[24] Vonk CG. J Appl Crystallogr 1973;6:148–52.
[25] Cao A, Ichikawa M, Kasuya KI, Yoshie N, Asakawa N, Inoue Y, et al. Polym J 1996;28:1096–102.
[26] Matsusaki H, Abe H, Doi Y. Biomacromolecules 2001;1:17–22.
[27] Gross RA, DeMello DC, Lenz RW, Brandl H, Fuller RC. Macromolecules 1989;22:1106–15.
[28] Preusting H, Nijenhuis A, Witholt B. Macromolecules 1990;23:4220–4.
[29] Koenig JL. Spectroscopy of polymers. Washington DC: American Chemical Society; 1992.
[30] Zhu B, He Y, Asakawa N, Nishida H, Inoue Y. Macromolecules 2006;39:194–203.
[31] Zhang J, Sato H, Tsuji H, Noda I, Ozaki Y. J Mol Struct 2005;735:249–57.
[32] Sato H, Murakami R, Zhang J, Mori K, Takahashi I, Terauchi H, et al. Macromol Symp 2005;230:158–66.
[33] Hu Y, Zhang J, Sato H, Noda I, Ozaki Y. Polymer 2007;48:4777–85.
[34] Sato H, Murakami R, Padermshoke A, Hirose F, Senda K, Noda I, et al. Macromolecules 2004;37:7203–13.
[35] Krimm S, Liang CY, Sutherland GBBM. J Chem Phys 1956;25:549–69.
[36] Li X, Hsu SL. J Polym Sci Polym Phy Ed 1984;22:1331–42.
[37] Quchi I, Hosoi M, Shimotsuma SJ. Appl Polym Sci 1977;21:3445–56.
[38] Hiroatsu M, Tatsuo M. J Polym Sci 1969;7:1735–44.
[39] Zhang J, Sato H, Noda I, Ozaki Y. Macromolecules 2005;38:4274–81.